



OTC 24642

Discrete Element Method Helps Determine Load Levels for Ice-Capable Jackups

Shaocheng Di, Shunying Ji / Dalian University of Technology;
Jiancheng (Jessie) Liu, Han-Chang Yu / American Bureau of Shipping

Copyright 2014, Offshore Technology Conference

This paper was prepared for presentation at the Arctic Technology Conference held in Houston, Texas, USA, 10-12 February 2014.

This paper was selected for presentation by an ATC program committee following review of information contained in an abstract submitted by the author(s). Contents of the paper have not been reviewed by the Offshore Technology Conference and are subject to correction by the author(s). The material does not necessarily reflect any position of the Offshore Technology Conference, its officers, or members. Electronic reproduction, distribution, or storage of any part of this paper without the written consent of the Offshore Technology Conference is prohibited. Permission to reproduce in print is restricted to an abstract of not more than 300 words; illustrations may not be copied. The abstract must contain conspicuous acknowledgment of OTC copyright.

Abstract

Ice-capable jackups can offer mobility and efficiency while drilling in shallow, ice-infested waters. However, the industry has limited experience operating jackups in ice environments, and technology gaps and uncertainties remain when assessing ice loads on multi-legged jackup units.

The Graphic Processing Unit (GPU)-based Discrete Element Method (DEM) can be applied to investigate the degree of ice effects on multi-legged jackup units. In previous applications, the DEM method was used to simulate ice interaction with structures, but computations were limited to simple interactions. Introducing a GPU platform enables a substantial increase in the number of elements characterized so that the interaction of multi-legs and ice can be modeled with greater efficiency. For example, level ice modeled with 3-D bonded spherical elements can address the buoyancy, current effects and drag force encountered in harsh environments. Additionally, the parallel bonding approach and de-bonding criteria are used to model level ice freezing and breakage.

In this investigation, the global ice loads on a jackup unit's single leg are analyzed to determine the effects of ice thickness, ice strengths and drifting velocities. The estimated ice loads are validated against full-scale data acquired from one application in Bohai Bay. Further, the mechanism of the interaction between the multiple legs and level ice is analyzed using the large-scale GPU-based simulation, the effects of sheltering and jamming are investigated and the ice loads simultaneously acting on the multiple legs are estimated to determine the total shear force and overturning moment.

Introduction

The ice-capable jackup is of interest for use in the shallow ice-infested waters due to its mobility and efficiency. However, the industry has limited experience in operating jackups in ice environments, and technology gaps and uncertainties remain in assessing ice loads on multi-legged jackup drilling units.

The existing standards/codes, ISO 19906, API RP 2N, CSA S471, Snip and VSN, provide the empirical ice force formulas for only simple ice-structure interactions; for example, the level ice acting on one continuous surface of the fixed structure. The global load prediction on jackups with open truss type legs is a challenging topic in the industry. ISO 19906 (2010) provides empirical formulas for assessing the ice loads on multi-legs based on physical model tests. The ice velocity, thickness and drift direction effects of the ice loads are not included. The jamming phenomena and effects to ice loads are discussed on a high level without the quantitative assessments. Moreover, the coefficients used in the formulas are based on physical model test results and uncertainties exist in determining their values during the design.

In recent years, the numerical approach has been further developed in solving the ice actions on marine/offshore structures (Derradji 2002, Gagnon 2011, Jorddan 2001, Karna 1999, Konuk 2009, Kuutti 2013, Sayed, 2012, Liu 2012, Wang, 2008). One numerical approach, the Discrete Element Method (DEM), has been successfully used for the simulation of ice interaction with offshore structures in previous studies (Di et al., 2012; Hopkins, 2013, Ji et al., 2013; Lau et al., 2011; Paavilainen et al., 2013). However, the high demand of computational resources has limited the application to simple

interactions. In this paper, the newly developed Graphic Processing Unit (GPU)-based DEM is applied to investigate the level ice actions on multi-legged jackup units. The use of the GPU platform allows modeling with a large number of elements so that the interaction of multi-legs and ice can be modeled efficiently. The level ice is modeled with 3-D bonded spherical elements considering buoyancy and drag force of the current. The parallel bonding approach and de-bonding criteria are adopted to model the freezing and breakage of level ice.

The global ice loads on a single leg is first investigated to address the effects of ice thickness and ice strengths. The GPU-DEM model estimated ice loads are validated against the full-scale data on a jacket in Bohai Bay. Both the ice load amplitude and frequency are compared between the measurements and simulation results. The level ice moving through two kinds of jackup legs, open truss type legs and cylindrical legs, were simulated using GPU-DEM model. The mechanism of the interaction between the multiple legs of the jackup and level ice is further investigated using the large-scale GPU-based simulations. The effects of sheltering and jamming are investigated with respect to the ISO 19906 standard. The ice loads simultaneously acting on the multiple legs are estimated to determine the total shear force and overturning moment.

The results from the numerical simulations based on the GPU-DEM model could serve as supplementary information to the standard/code-based ice load assessments when designing the structure of the jackup.

GPU-DEM Model of Ice

The DEM model is able to reasonably simulate the micro-mechanical properties of ice as well as the macro ice breakages caused by interaction with the structure. However, due to the limitation of the computational capacity of a typical CPU, the DEM model adopting the use of serial-computation technology cannot be extended to the large scale; therefore, only the simple ice-structure interactions were simulated in the past. GPU-based DEM software adopts parallel computation technology and can be utilized to model a large number of elements, thus providing a highly efficient approach for simulating the complicated interactions between the ice and the offshore structures.

In the DEM simulations, the sea ice model consists of the bonded spherical elements with masses and sizes. The bonding between spherical elements can be fractured under the external forces [Ji et al., 2013]. Figure 1 presents the contact models between elements and bonding fracture criterion (Paavilainen et al., 2011). The adopted linear-softened fracture criterion satisfies the below equation,

$$f(F_i, \delta_{\max}) = F_i - F_{i_{\max}} (1 - \delta_{\max} / \delta_f) = 0 \quad (1)$$

Where, $F_i (i = n, s)$ are the normal contact forces and shear contact forces. $F_{i_{\max}}$ are the maximum normal contact forces and shear contact forces. In Figure 1, δ_{crit} is the maximum displacements caused by the maximum normal forces and the shear contact forces. δ_{\max} is the maximum normal displacement and shear displacement before the offloading, $\delta_{\max} > \delta_{\text{crit}}$; δ_f is the maximum normal displacement or shear displacement when the bonding is fully broken.

When the fracture criterion, $f < 0$, the bonding between the elements is intact or the bonding breakage exists but with no propagation. When the fracture criterion, $f = 0$, the bonding between particles is to be broken or at the offload status. In Figure 1, K_1 is the normal contact stiffness or shear contact stiffness between elements. K_2 is the linear softening contact stiffness. Their values can be determined by the ratio of δ_f and δ_{crit} . Here, $\delta_f = 1.5\delta_{\text{crit}}$.

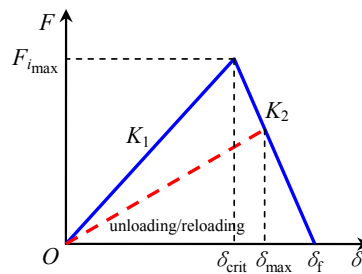


Figure 1 Linear softening contact model of fracture of bonded elements

Contact Detection between Ice and Jackup

A jackup operating in Bohai Bay is selected for the calculation examples in this paper, as shown in Figure 2. Figure 3 presents the DEM model of the jackup's leg. The model does not consider the effects from the gear racks to the ice actions on the legs.



Figure 2 Jack-up in Bohai Bay

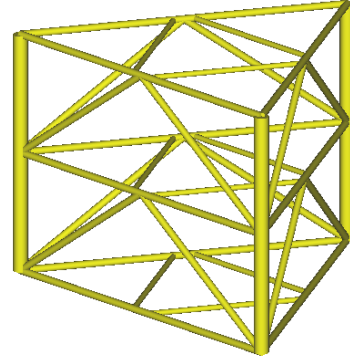


Figure 3 DEM model of the jack-up leg

The open truss-type leg consists of the cylindrical column members. The contacts between spherical element and the cylindrical structure have three primary types, as shown in Figure 4.

- (a) contact between spherical element and the side surface;
- (b) contact between spherical element with the flat bottom/top surface;
- (c) contact between the spherical element and the edges.

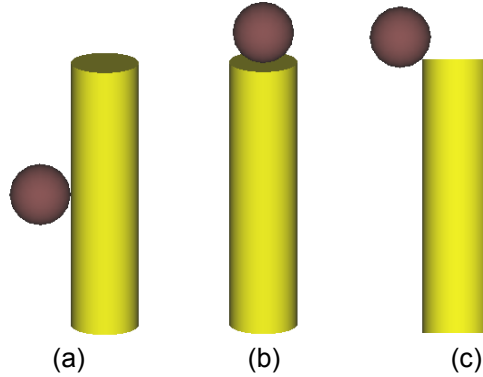


Figure 4 Contact modes between sea ice element and cylindrical structure

In order to judge the contact between ice element and cylindrical structure, some specific points are first defined: the circle centers of two base surfaces, A and B, radius, $R_{cylinder}$, position of cylinder center, P, and radius of spherical element, R_{ball} . The projection of the point P at the axis of the cylinder is Q, as shown in Figure 5 (a-c). The below vectors connecting those points are then acquired, AP 、 BP 、 AB 、 BA 、 BQ and QP . Where, $BQ = BP - QP$, $QP = AP - \frac{AP \cdot AB}{|AB|} \cdot \frac{AB}{|AB|}$.

The contact detection for the spherical element and cylindrical structure include three ways:

- (a) The contact between the spherical element and the side surface
The center of spherical element is first checked as to whether it is in the area A1, as shown in Figure 5(a). If $(AP \cdot BA)(BP \cdot BA) \leq 0$, then the element is in the area A1 and the contact between element and cylinder is further checked. If $|QP| < R_{cylinder} + R_{ball}$, then the element contacts with the cylinder.
- (b) The contact between the spherical element and base surfaces
If $(AP \cdot BA)(BP \cdot BA) > 0$, then the spherical element is in area A2 or A3, as shown in Figure 5(b); If $|QP| < R_{cylinder}$, then the spherical element is in area A2; if $|BQ| < R_{ball}$, then the element contacts the base surface of cylinder.
- (c) The contact between the spherical element and the cylinder edges
If $(AP \cdot BA)(BP \cdot BA) > 0$ and $|QP| > R_{cylinder}$, then the spherical element, P, is in area A3, as shown in Figure 5(c). If P is at the cylinder edge, then there are the following two relationships, $BN = R_{cylinder} \cdot QP / |QP|$ and $NP = BP - BN$. If

$|NP| < R_{\text{ball}}$, the spherical element, P, contacts with the cylinder edge.

The overlap length between element and cylinder is calculated in order to calculate the contact force based on the corresponding contact force models (Ji et al., 2013).

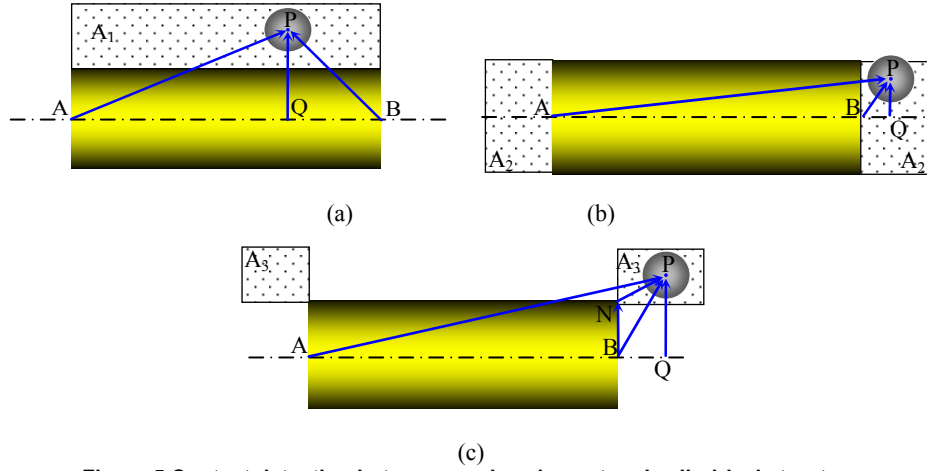


Figure 5 Contact detection between sea ice element and cylindrical structure

The two kinds of jackup legs, the open truss-type legs and the cylindrical legs, are considered in the simulations of level ice and jackup leg interactions. Obviously, the ice contact modes for the open truss-type leg can be used in simulating the interactions between the ice and the cylindrical leg.

GPU-based DEM Algorithms for Parallel Computing

In this algorithm, the neighbour list method is adopted to establish the contacts between the particles (Nishiura et al., 2011). The simulated ice region is divided into several cells, whose dimensions are slightly larger than the diameters of the particles, so that the particle only contacts with the particles within the cell and neighbor cells. Therefore, only twenty-seven neighbor cells including the cell this particle belongs to are to be searched to generate the neighbor list. After the establishment of neighbour list, the contact force between particle pairs will be calculated according to the Newton's equation of motion, and the whole procedure is shown from steps 1 to 6.

(1) First, the particles are presorted according to the cell index to which the particles belong; Figure 7(a) illustrates the state of the particles after sorting and re-indexing of the particles as shown in Figure 6. Next, the maximum and minimum particle index in each cell, $I_p^{\min}[I_{\text{cell}}]$ and $I_p^{\max}[I_{\text{cell}}]$, will be obtained as shown in Figure 7(b), where I_{cell} is the index of cells.

(2) Generate the neighbor array of the particle, i , $A_{\text{nei}}[i, I_{\text{nei}}]$. The value of I_{nei} is between 0 and $N_{\text{max}} - 1$, N_{max} is the maximum number of the particles contacting with the particle i . In this paper, the equal-sized elements are used, so each particle can contact with at the most 12 neighbor particles. In the neighbor list of the particle, i , the number of neighbour particles with index bigger than i is $n_{\text{jgi}}[i]$.

(3) The prefix sum is computed for the neighbour particles $n_{\text{jgi}}[i]$ using the below equation,

$$s_{\text{jgi}}[i] = \sum_{n=0}^i n_{\text{jgi}}[n] \quad (2)$$

Then, the index, I_{list} , of the contact candidate pair list is given by the equation,

$$I_{\text{list}} = s_{\text{jgi}}[i-1] + I_{\text{nei}} \quad (I_{\text{nei}} \in 0, n_{\text{jgi}}[i]-1) \quad (3)$$

(4) Generate neighbor lists, L_p and L_n , using the algorithm given in Table 1.

Table 1 Generation of neighbor list

Algorithm: Generate neighbor list
1: for $i = 0$ to $N_p - 1$ (Loop for all particles, N_p is sum of the particles)
2: for $I_{\text{nei}} = 0$ to $n_{\text{jgi}}[i] - 1$
3: $I_{\text{list}} \leftarrow s_{\text{jgi}}[i-1] + I_{\text{nei}}$ (equation 3)

```

4:    $j \leftarrow A_{nei}[i, l_{nei}]$ 
5:    $L_p[l_{istd}] \leftarrow i$ 
6:    $L_n[l_{istd}] \leftarrow j$ 
7:   end do
8: end do
    
```

(5) Calculate the contact force. The contact forces between particles due to the overlap between the two particles are calculated (Ji & Di, 2013; Ji & Li, 2013). If two particles contact at the current and next time step, the contact force between the two particles is transferred from current time step to next time step. That process is repeated among all neighbor elements.

(6) Update the coordinates of the particles. Based on the total forces on the particle, the velocity and position of the particle are calculated according to Newton’s second law.

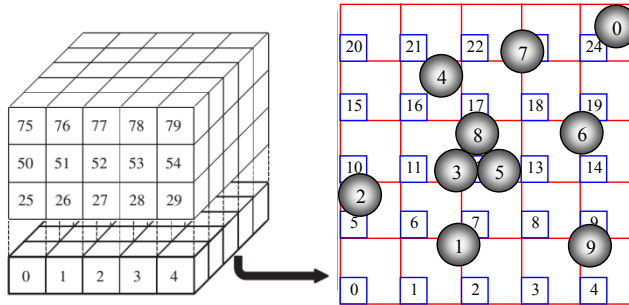


Figure 6 Particle position in space grid

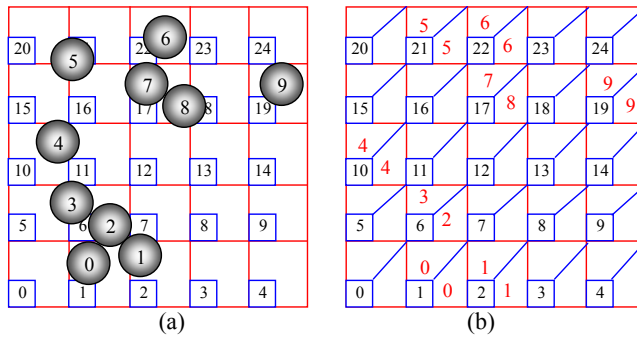


Figure 7 Sorted particle and the maximum and minimum particle indexes in each cell

In this paper, the discrete element algorithm is built up at the NVIDIA Tesla K20 platform. This GPU consists of 13 Streaming Multi-Processors (SMX). Each SMX contains 92 single precision computing units, 64 double precision computing units and other function units. Within the CUDA programming, the threads are organized to three levels: grid, blocks and threads. The computation of the contact force between two particles in neighbour list will be carried out on each thread, and every thread block consists of 256 threads. After the calculation on GPU, the results will be copied from Device (GPU) memories to Host (CPU) memories, and the positions, velocities and angle velocities of all particles can be output.

Validation of DEM model Using Bahai Bay Jacket Data

The DEM model was validated using the field data measured on one leg of Bohai Bay Jacket (Wang et al., 2012), JZ20-2 MUQ B2, as shown in Figure 8(a). The leg has an installed cone to break the level ice in flexural as shown in Figure 8(b). The geometries of the jacket cone and the mass of the jacket were used in the simulation. The stiffness of the pile is calculated from the real leg structures. Ice thickness, velocity and other environmental data were measured in the field. In the model, finite level ice is used to model the infinite ice, and the in-plane resistance on the modeled ice sheet edges from far-field level ice was represented using springs. The parameters of the DEM model in the simulation are listed in Table 2.

The physical process of the level ice being broken by the conical leg of the jacket was simulated using the GPU-based DEM model as shown in Figure 9. It is observed that the DEM model simulates the phenomenon of the cone breaking the ice sheet into the ice blocks due to the flexural bending failure with reasonable accuracy as shown in Figures 8(b) and 9.

Figure 10 presents the comparisons of the DEM simulated and field-measured ice load time histories on the JZ20-2MUQ leg. The maximum ice load in field measurement is 117kN, and the maximum ice load in simulation is 124kN. The frequency of maximum ice force in the field test is about 1.7 seconds and 1.9 seconds in the simulation. It can be seen that the simulation results agree fairly well with the measurements across several ice load amplitudes and frequencies. Only the global ice load on the structure is validated based on the field data, considering that at the thin ice sheet, the ice loads from the full ice thickness is used for the Jackup structural design. The Jackup is not likely to be impacted by a massive ice feature and therefore local ice pressure by such a feature is not included in the current GPU-DEM model-based study.

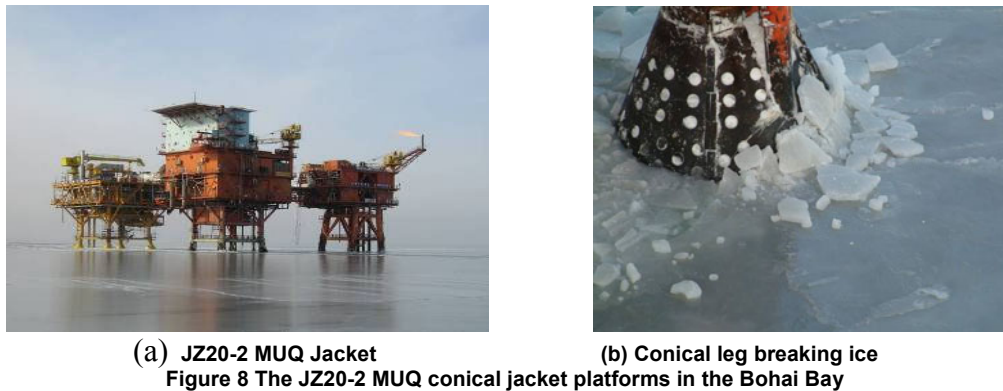
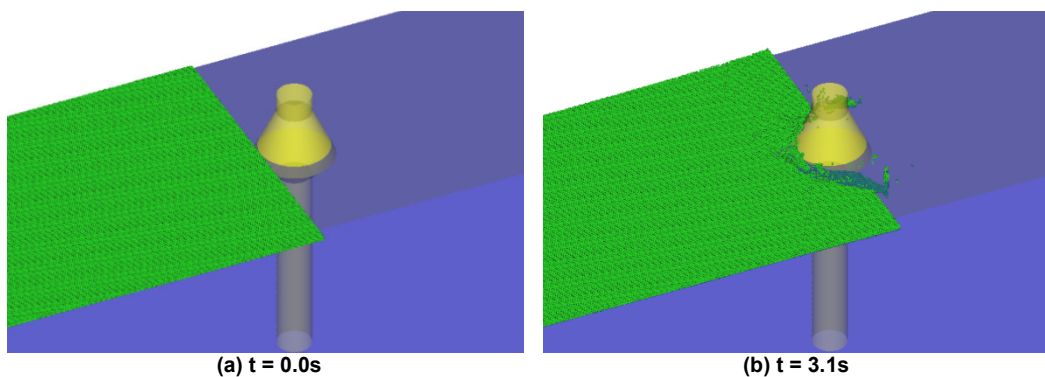


Table 2 Main Parameters of GPU-DEM Model for the Level Ice Action on Conical Leg

Items	Symbol	Unit	Values
Water density	ρ_w	Kg/m ³	1035
Drag coefficient	C_D		0.005
Current velocity	V	m/s	0.43
Ice Density	ρ_i	kg/m ³	920
Ice sheet size	$L \times W$	m	20×15
Ice thickness	t_i	m	0.23m
flexural strength	σ_f	MPa	1.5 MPa
Uniaxial compressive strength	σ_c	MPa	3.0MPa
Partical Diameter	D	m	0.09
Waterline Diameter of cone	D_L	m	2.85
Sloping angle of cone	α	deg	65



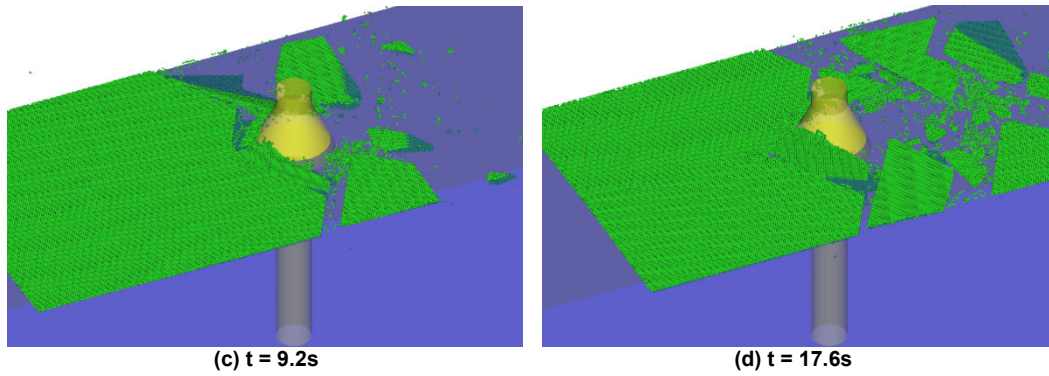


Figure 9 Interaction between sea ice and conical pile simulated with DEM

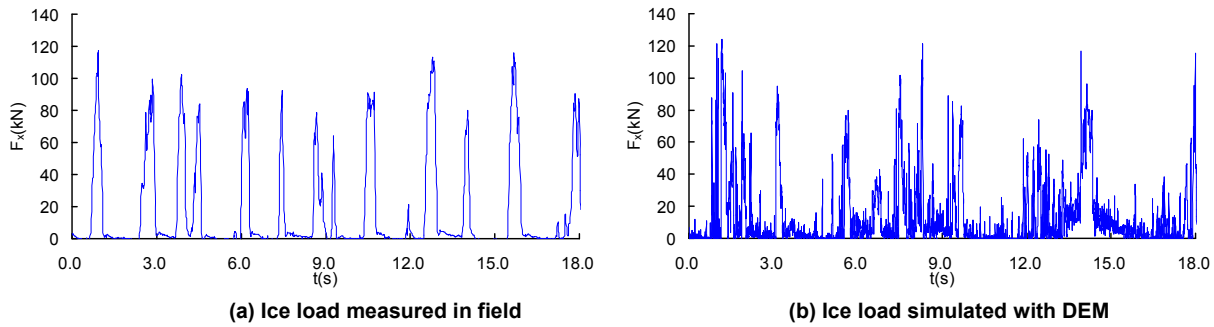
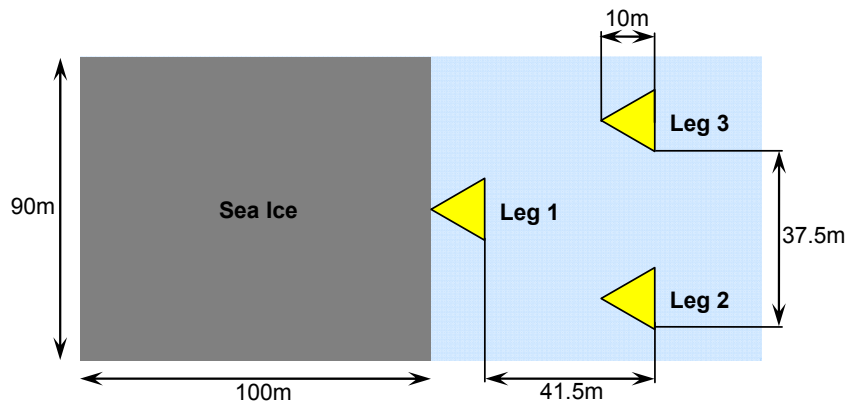


Figure 10 Comparison of ice loads obtained from the field measurement and DEM simulation

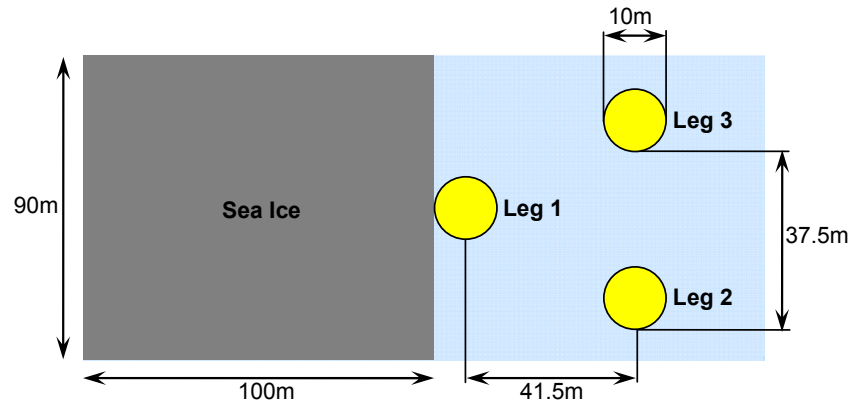
Level Ice Actions on Multiple Legs of Jackup

Figure 12 presents the scenarios of the level ice and the jackup interaction for the simulations. The jackup examples have two kinds of legs, three triangular open-truss legs and a tri-cylinder leg. The ice breakage and the resulting force time histories on the jackup legs were simulated using a DEM model. Table 3 lists the parameters of the DEM model. In the simulations, the jackup is modeled as a rigid body fixed on the sea bed. The drag forces on the ice from the current were calculated using the Morison theories (Sun & Shen, 2012). The ice sheet is moved forward by defining the ice sheet edge further away from the legs with a constant velocity, 1.0m/s.

A 75-second duration of the level ice sheet and Jackup interaction was simulated in the calculation examples, requiring 100 hours running time on the K20 GPU Card workstation.



(a) The level ice acting on the triangular open-truss type legs



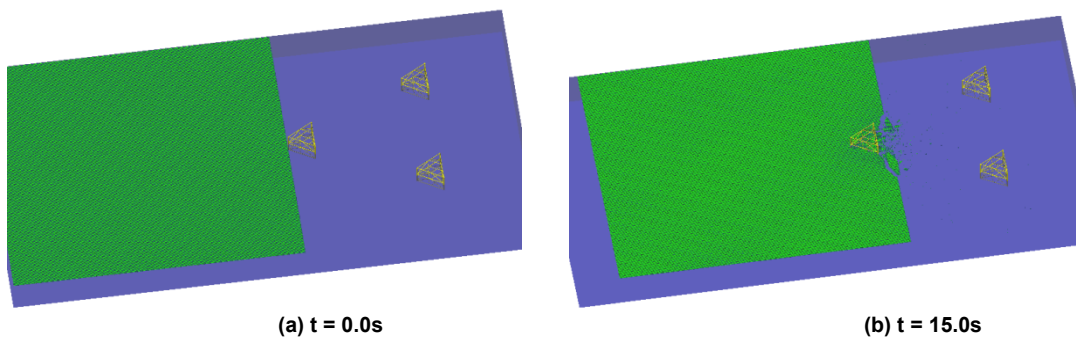
(b) The level ice acting on the cylinder legs
 Figure 12 Sketch of the interaction between sea ice and jack-up platform structure

Table 3 Main parameters of the DEM model for the Level Ice Action on Jackup Legs

Items	Symbol	Unit	Value
Water density	ρ_w	kg/m ³	1035
Drag coefficient	C_D		0.005
Current velocity	V	m/s	1.0
Ice density	ρ_i	kg/m ³	930
Ice thickness	h	m	0.5
Ice sheet size	$a \times b$	m ²	100×90
Uniaxial compressive strength	σ_c	MP _a	2.0
Flexural strength	σ_f	MP _a	0.85
Particle diameter	D	m	0.25
Particle number	N_p		3.32×10^5

Figure 13 shows the simulated physical process of level ice moving through three triangular open-truss type legs. In the simulation results, the green regions represent the ice and the blue regions the sea water. It can be seen that the channel edge left by the front leg has obvious effects on the ice breaking process at the rear legs. In the simulation results, no jamming between legs was observed. The ice sheet in direct contact with the legs is broken into small pieces. The ice sheet between the front leg and the rear legs is split into large pieces; those large ice floes may be jammed at the rear legs as shown in Figure 13 (d).

The ice force time histories on the jackup legs are presented in Figures 14-16. Table 4 lists the maximum forces and mean forces on the legs. The front leg experienced higher loads than the rear two legs. The front leg shielded the rear legs, the channel left by the front leg frees the boundary condition of the ice sheet to be broken by the rear legs. The ice load on the front leg is mainly in the x direction, which is the sea ice attack direction. The mean ice force in the y direction has a small value which is caused by the asymmetric failure of the ice beside the leg and the characteristics of the DEM model: the small spherical elements and the calculation errors.



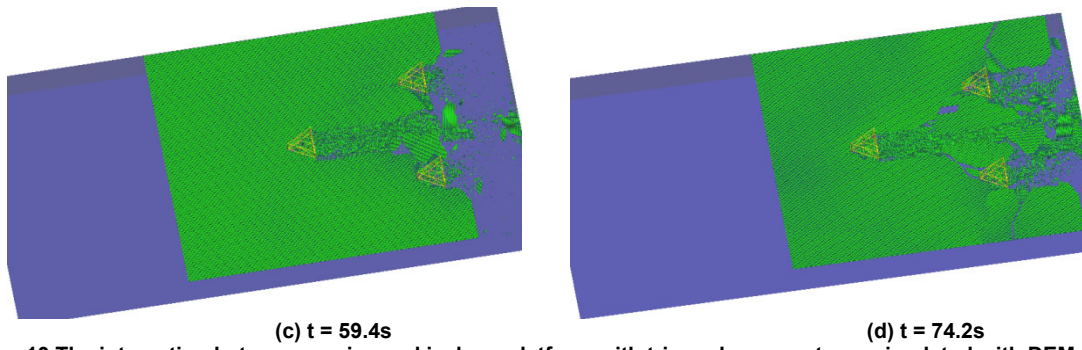


Figure13 The interaction between sea ice and jack-up platform with triangular open- truss simulated with DEM

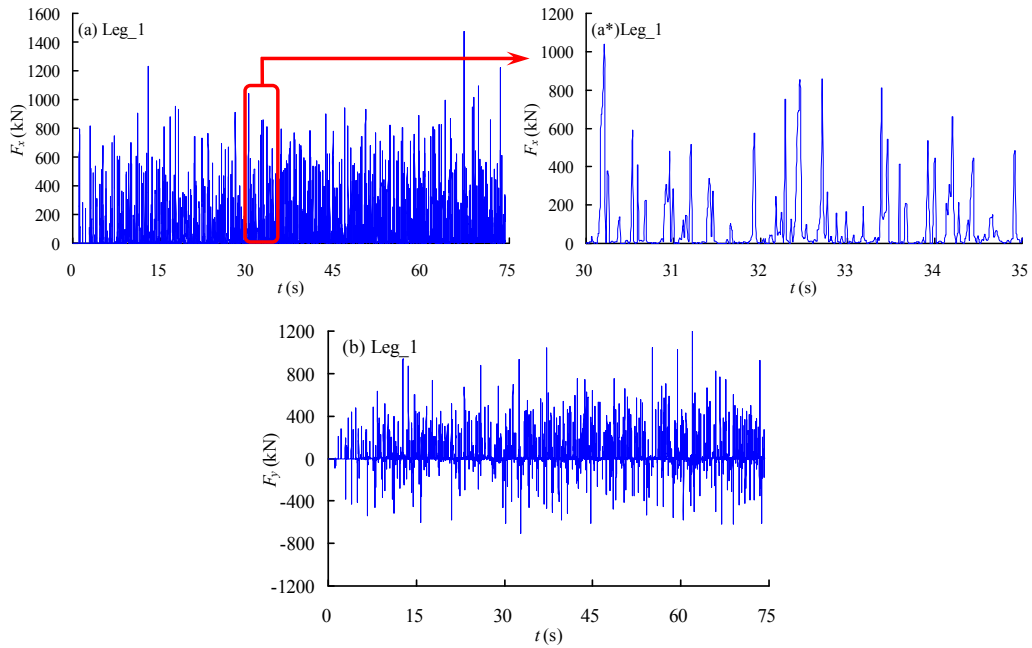


Figure 14 Ice load time histories of leg 1 simulated with DEM

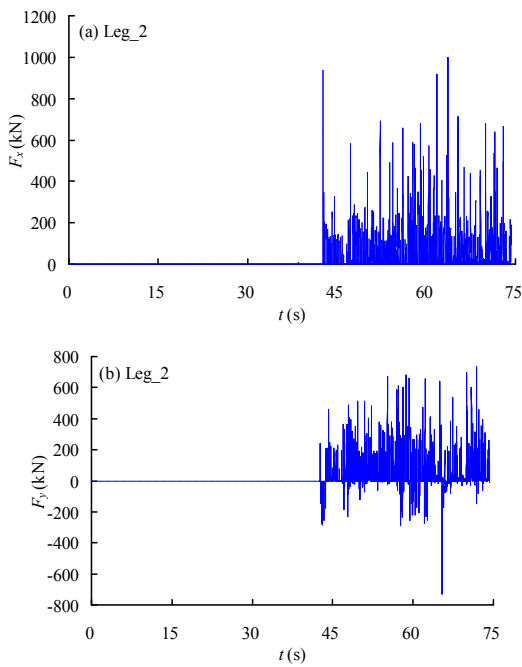


Figure 15 Ice load time histories of leg 2 simulated with DEM

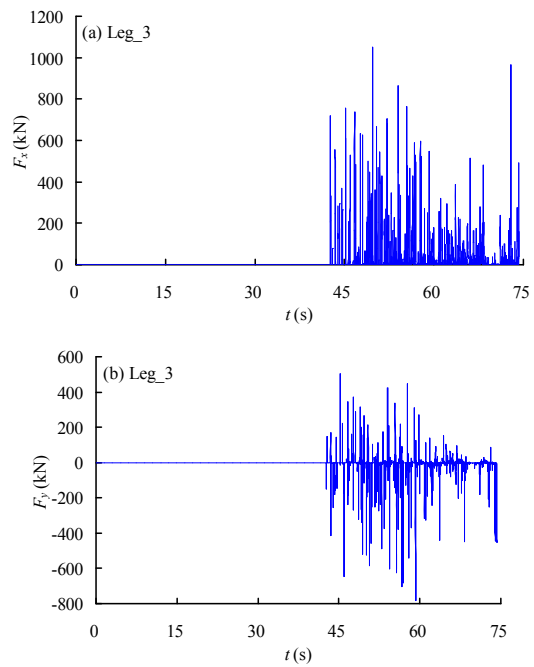
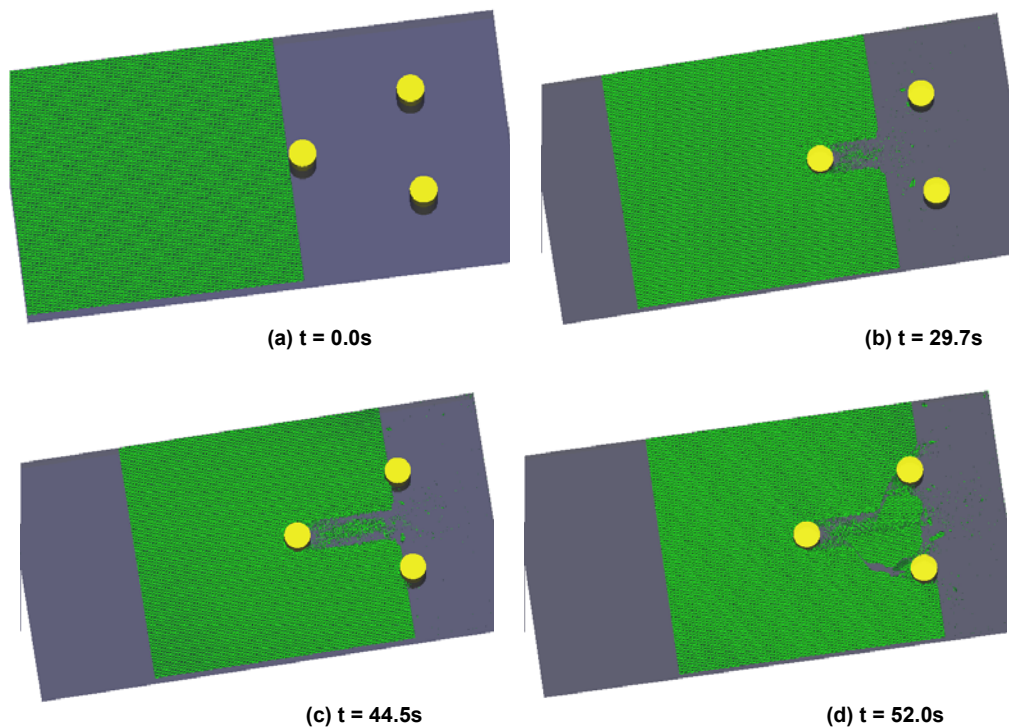
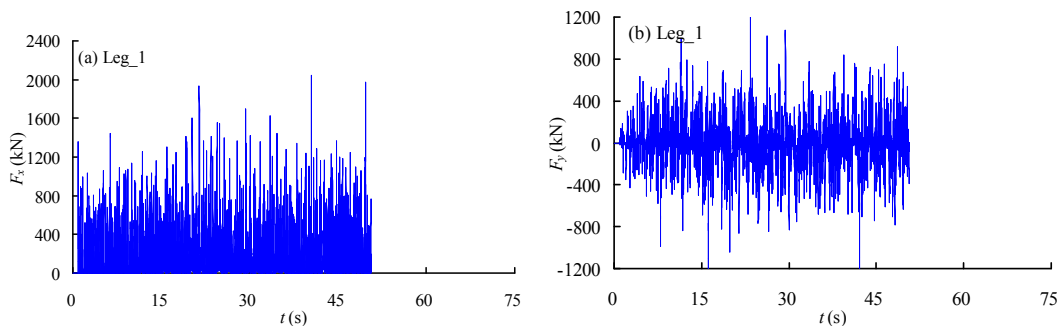


Figure 16 Ice loads time histories of leg 3 simulated with DEM

Table 4 Ice loads on the legs calculated using DEM model

Jackup		1#	2#	3#
Max (kN)	x	1475	1001	1050
	y	1261	738	503
Mean (kN)	x	80	36	31
	y	28	27	-9.8

Figure 17 presents the simulated physical process of the level ice sheet moving through tri-cylinder legs of the jackup. The ice force time histories on the jackup legs are presented in Figures 18-20. Table 5 lists the maximum ice forces and mean ice forces on the legs. A similar ice breaking process as seen with the tri-open truss type legs is observed. The global maximum forces and global mean forces on the cylindrical legs are slightly larger than the corresponding loads on the open trussed legs, however this does not mean that the open trussed leg is better at resisting the ice loads than the cylindrical legs. The small diameter, weak members of open truss type legs directly contact the level ice and can be damaged by the high local ice loads, which may consequently result in the global collapse of the legs. The local ice loads on the structures and effects on the scantling design are beyond the scope of this paper and will be presented in future publications.

**Figure17 The interaction between sea ice and jack-up platform with tri-cylinders simulated with DEM****Figure 18 Ice load time histories of leg 1 simulated with DEM**

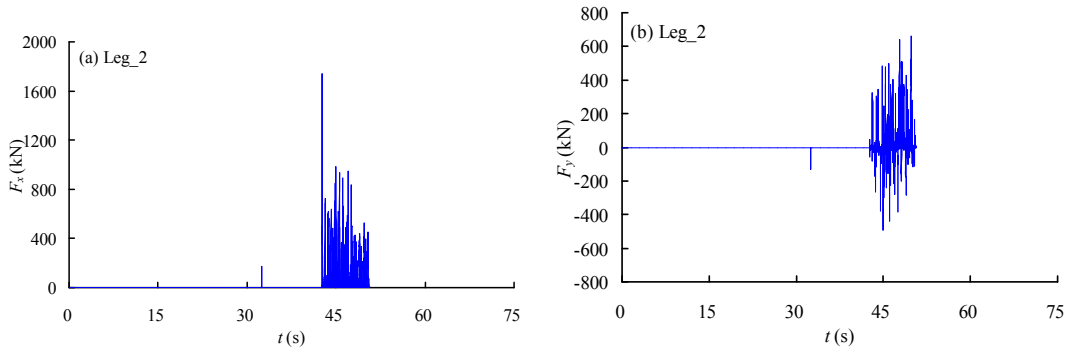


Figure 19 Ice load time histories of leg 1 simulated with DEM

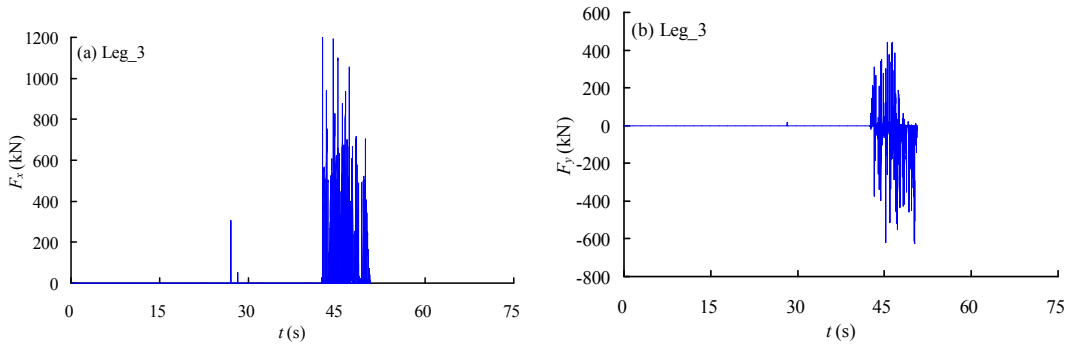


Figure 20 Ice load time histories of leg 1 simulated with DEM

Table 5 Ice loads on the legs calculated using DEM model

Jackup		1#	2#	3#
Max (kN)	x	1915	1373	1650
	y	1238	800	531
Mean (kN)	x	173	32	38
	y	16	17	-17

Conclusions and Recommendations

This paper introduced the newly developed GPU-based DEM model in Dalian University of Technology (DUT), China, which adopts parallel computation technology and can calculate the large-scale DEM model required for simulating the complicated ice-structure interactions, such as a level ice sheet moving through the multiple legs of a jackup.

The validation of the GPU-DEM model using the field data of ice-structure interactions is an important and essential step to allow numerical prediction of the ice loads on structures. In the paper, the field data of level ice sheet acting on the conical leg of Bohai Bay Jacket, JZ20-2 MUQ B2, were first used in validating the GPU-DEM model. The validation includes visual comparisons of the ice-cracking process and quantitative comparisons of the ice load amplitudes and frequency. Good agreement between field measurements and simulation results were achieved.

The physical processes of the level ice moving through the jackup’s multi-legs were simulated using the GPU-DEM model. The ice sheet breakage and ice floes drifting through the legs were visually observed and discussed. The predicted ice loads on the three legs were analyzed. Through qualitative comparison with existing knowledge and industry experience, it can be concluded that the simulation results using the GPU-DEM model were reasonable for the analysed scenario, a level ice sheet moving through multiple legs. The quantitative validation of the DEM model in calculating the ice load on the multiple legs requires additional data from model experiments and full-scale measurements, which was not presented in this paper.

This work presented in this paper verified the promising future of applying the GPU-DEM model in simulating the complicated interactions between level ice and multiple-legged jackups and predicting the ice loads. Further work will include assessing the ice loads on jackup rigs under different ice conditions using the GPU-DEM model, including ice velocity, ice thickness, ice direction, ice sheet size and boundary conditions. The flexibility of the jackup rig during the dynamic ice actions can be modeled by redefining the mass of the leg model and using equivalent springs connecting the leg model and seabed. In theory, the GPU-DEM model has the capability to simulate the interaction between the structure and the multiple types of ices, i.e. pack ices, FY ridge ice, rubble ice, etc. The further validation of the DEM model based on the

additional data, full-scale data and model-scale data will be carried out in the DEM model developments.

Acknowledgements

The authors gratefully acknowledge the support of James Bond of the American Bureau of Shipping (ABS). The authors also wish to express their appreciation to ABS management for their support of the paper's publication.

References

- API, 1995, Recommended Practice for Planning, Designing, and Constructing Structures and Pipelines for Arctic Conditions, API RP 2N.
- CSA, 2005, General Requirements, Design Criteria, the Environment, and Loads, A National Standard of Canada, CSA S471-04.
- Di S, Ji S, Yue Q, Liu S. 2012, Ice Loads on Conical Offshore Structures Based on Discrete Element Simulation, Proceedings of 21st IAHR International Symposium on Ice, Dalian, China.
- Derradji-Aouat A., 2002, Multi-surface failure criterion of saline ice in the brittle regime, *Cold Regions Science and Technology*, 36, 47-70.
- Gagnon R., 2011, A numerical model of ice crushing using a foam analogue. *Cold Regions Science and Technology*, 65: 335–350.
- ISO, 2010, Petroleum, and Natural Gas Industries – Arctic Offshore Structures, ISO 19906
- Jordaan I., 2001, Mechanics of ice-structure interaction. *Engineering Fracture Mechanics*, 2001, 68: 1923–1960.
- Ji S., Di S., Li Z., Bi Xi, 2013, Discrete Element Modelling of Interaction between Sea Ice and Vertical Offshore Structure, *Engineering Mechanics*, 30(1) 463-469.
- Ji S, Li Z, Liu S., 2013, Discrete element simulation of ice loads on an up-downward cone. The 6th International Conference on Discrete Element Methods (DEM6), Golden, USA.
- Hopkins M., 2013, Discrete Element Sea Ice Modelling, Proceedings of the 22nd International Conference on Port and Ocean Engineering under Arctic Conditions, June 9-13, Espoo, Finland.
- Kärnä T, Kamesaki K, Tsukuda H. 1999, A numerical model for dynamic ice-structure interaction. *Computers and Structures*, 72: 645–658.
- Konuk I, Gürtner A, Yu S. A., 2009a, Cohesive element framework for dynamic ice-structure interaction problems - part I: review and formulation. Proceedings of the ASME 2009 28th International Conference on Ocean, Offshore and Arctic Engineering, Hawaii, USA OMAE2009-79262
- Kuutti J, Kolari K, Marjavaara P. 2013, Simulation of ice crushing experiments with cohesive surface methodology. *Cold Regions Science and Technology*, 92: 17–28
- Lau M, Lawrence K P, Rothenburg L. 2011, Discrete element analysis of ice loads on ships and structures. *Ships and Offshore Structures*, 6(3): 211–221
- Liu J., Daley C., Yu H., Bond J., 2012, Comparison of Analytical and Numerical Models of Glancing Ship-Ice Collisions, *Icetech'12*, Banff, Canada.
- Nishiura D, Sakaguchi H., 2011, Parallel-vector algorithms for particle simulations on shared-memory multiprocessors [J]. *Journal of Computational Physics*, 230: 1923-1938.
- Paavilainen J, Tuhkuri J. 2013, Pressure distributions and force chains during simulated ice rubbing against sloped structures. *Cold Regions Science and Technology*, 85: 157–174
- Paavilainen J, Tuhkuri J, Polojärvi A. 2011, 2D numerical simulations of ice rubble formation process against an inclined structure [J]. *Cold Regions Science and Technology*, 68: 20-34.
- Palmer A, Yue Q, Guo F., 2010, Ice-induced vibrations and scaling. *Cold Regions Science and Technology*, 60: 189–192.
- Polojärvi A, Tuhkuri J., 2009, 3D discrete numerical modelling of ridge keel punch through tests. *Cold Regions Science and Technology*, 2009, 56: 18–29.
- Selvadurai A P S, Sepher K., 1999, Two-dimensional discrete element simulations of ice-structure interaction. *International Journal of Solids and Structures*, 36: 4919–4940.
- Sayed M., Kubat I, Wright B., Iyerusalimkiy S, Phadke A., Hall B., 2012, Numerical Simulation of Ice Interaction with a Moored Structure, *Icetech'12*, Banff, Canada.

SNiP, 1995, Loads and Effects on Hydrotechnical Facilities (Caused by Waves, Ice, Vessels), Construction Codes and Regulations, Moscow, SNiP 2.06.04-82.

Sun S., Shen H., 2012, Simulation of Pancake Ice Load on a Circular Cylinder in a Wave and Current Field, Cold Regions Science and Technology, 78(2012) 31-39.

VSN, 1988, Design of Ice-Resistant Stationary Platforms, Ministry of the Oil Industry of the USSR, Moscow, VSN 41.88.

Wang Y, Yue Q, Guo F, et al., 2012, Performance evaluation of a new ice-resistant jacket platform based on field monitoring. Cold Regions Science and Technology, 71: 44–53.

Wang Gang, Wu Wen-hua, Yue Qian-jin, 2008, FEM analysis on ice-bending failure mode with width effect of ice-cone interaction. Engineering Mechanics, 25(1): 235–240.